

# The relationship between ionic activities and temperature in $\text{Li}_2\text{Na}_2\text{MnO}_4$ material

O. MURAT OZKENDIR\*

Department of Mathematical and Natural Sciences, Tarsus University, 33400, Tarsus, Turkey

In order to investigate the structural behaviours of  $\text{Na}_4\text{MnO}_4$  and lithium substituted  $\text{Na}_4\text{MnO}_4$  materials ( $\text{Li}_2\text{Na}_2\text{MnO}_4$ ) under conditions of increasing temperature, and to determine whether or not they possess the necessary characteristics to be a candidate for battery cathode, these materials' electronic and crystal structure properties were studied at temperatures of 300 K, 323 K, 343 K, 373 K, and 423 K. Studies on the electronic structure have shown that lithium substituted compounds and their parent materials both exhibit a stable electronic structure at high temperatures. The alkali metals (Na and Li) and also Mn are strongly linked to the oxygen atoms in the crystal, as evidenced by the durability of the crystal structure. Although the examined materials lacked the necessary qualities to serve as a battery cathode, the high electronic data loss with rising temperatures suggested that they may have good thermoelectric capabilities at room temperature with an unaffected, stable crystal structure. The outcomes of study are very compatible with the research reported in the literature.

(Received November 2, 2022; accepted June 9, 2023)

**Keywords:** Batteries, Electronic structure, Crystal structure, XAFS

## 1. Introduction

Energy storage device scientists are highly motivated to produce performance results that are superior to those now used in technology-driven utilities. Highly effective and less expensive batteries with stable capacities in the real world or in space have become more crucial recently with the rising prices of energy production and storage. As a result of sodium's greater abundance in the earth's crust and ease of manipulation, researchers studying lithium-ion batteries are concentrating on sodium-based batteries [1, 2]. The sodium ion batteries (SIB) still have a low working capacity despite having a number of advantages over lithium ion batteries, including lower cost, abundance, high energy density, greater cycle life, and improved cycling stability. There are also frequent problems that have not been solved, such as ionic loss with increasing cycles and capacity loss from the heat emitted during intercalation [1-3]. Actually, the history of SIBs predates that of lithium ion batteries (LIB), and they were initially explored in the 1970s, much like LIBs, before research on sodium type batteries was disregarded in favour of LIBs [4].

The manganese sodium oxosalt  $\text{Na}_4\text{MnO}_4$  is believed to be stable and is produced at 240 °C by the reaction of  $\text{Na}_4\text{MnO}_3$  and  $1/2\text{O}_2$ . In the sketched crystal structures shown in Fig. 1, a sodium oxide material's non-availability as a candidate for SIBs is clearly visible.  $\text{Na}_4\text{MnO}_4$  crystallises in triclinic geometry with the "P -1" space group. Fig. 1 (a) and Fig. 1 (b) make it clear that oxygen atoms securely encircle both the sodium and manganese atoms, making them more stable against internal and external influences. Tetrahedral features of the atomic sites, particularly in Fig. 1.b, make it very evident how closely oxygen atoms interact with metals (Mn and Na). This is

not a good property for batteries because, during the intercalation process, sodium atoms should detach themselves upon the application of a potential difference on the cathode part when connected to the anode, and should return to their older sites when the opposite potential is applied. Fig. 1 (b) makes the influence of oxygen atoms on the metals (Na and Mn) clearly obvious. Oxygen is a crucial component in creating crystals because of its strong electronegativity, which bonds metals like mortar between bricks.  $\text{Na}_4\text{MnO}_4$ 's resistance to external influences generated unpopularity and hasn't been studied, notably as a battery cathode.

In this study, real-space multiple scattering XAFS computations using the FEFF 8.20 algorithm are used to conduct electronic structural analyses [5]. 50% Li atoms were substituted for Na atoms in  $\text{Na}_4\text{MnO}_4$  to investigate how the ionic activity changed.

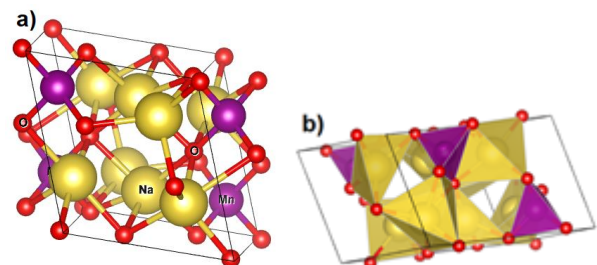


Fig. 1. (a) Triclinic "P -1" image of the  $\text{Na}_4\text{MnO}_4$  crystal (b) Tetrahedral image of the crystal [6] (color online)

Finding out whether or not lithium substitution affects the atomic coordination and weakens the oxygen bonds on the Li/Na atoms is the main objective of this study.

XAFS calculations, a potent method that produces information on crystal structure, electronic structure, and magnetic ordering, were used to conduct the experiments. Rich information on the chemical bonds between the interested atom and its neighbours, the interested atoms' electronic localization, and the excited atom's interstitial potential environment can be found in the electronic structure data of XAFS spectra. The extended XAFS (EXAFS), which is created by extracting the fluctuating data from the tail of the XAFS spectra, and the XANES (x-ray absorption near edge, or XAS) spectrum should be treated separately from each other. Actually, there are some similarities between XAFS and XAS (x-ray absorption spectroscopy). The spectra with variations coming from the scattering mechanism, which is located just beyond the XANES section, are what make the difference. The scattering intensity "chi" ( $\chi$ ), which can be retrieved from the gathered EXAFS data and calculated using a formula, is used to identify the atomic distance and positions from the source atom;

$$\chi = [\mu(E) - \mu_0(E)] / \Delta\mu_0 \quad (1)$$

In the formula,  $\mu$  is the absorption coefficient, where  $\mu_0$  is the sole atom's absorption coefficient. With other experimental parameters, the formula gives the chi signal of the photoelectrons, which can also be estimated from, (the EXAFS equation);

$$\chi(k) = \sum [(N_j f_j(k) \exp(-2k^2 \sigma_j^2)) / (k R_j^2)] \sin[2kR_j + \delta_j(k)] \quad (2)$$

In this equation, "N" is the coordination number of the neighbouring atom, " $f_j(k)$ " is the scattering amplitude, " $\delta_j(k)$ " is the scattering phase shift, "R" is the distance of the neighbouring atom, and " $\sigma_j^2$ " is the mean-square disorder with the neighbouring atom distances [7].

## 2. Materials and methods

$\text{Na}_4\text{MnO}_4$  and  $\text{Li}_2\text{Na}_2\text{MnO}_4$  crystals' crystal structures and electronic structural characteristics were examined by XAFS calculations with increasing heat treatment, utilising the real space multiple scattering method and the FEFF 8.20 algorithm [5]. The input file "feff.inp" used by the "Ab-initio" FEFF 8.20 algorithm contains initial settings for electronic energy information, crystal data, and environmental circumstances. TkAtoms was used to create the input files for the calculations [8–10]. A 10 angstroms thick cluster of 162 atoms (Na, Mn, and O) in the  $\text{Na}_4\text{MnO}_4$  crystal with the crystal characteristics of the triclinic "P-1" space group was created as the input file for the calculations:  $a = 5.6417 \text{ \AA}$ ,  $b = 5.8988 \text{ \AA}$ ,  $c = 8.6745 \text{ \AA}$ ,  $\alpha = 87.4712^\circ$ ,  $\beta = 108.9645^\circ$ ,  $\gamma = 111.9221^\circ$ .

The atomic coordinations are:

$$\text{Mn} (x:0.1045, y:0.7822, z:0.7560),$$

$$\begin{aligned} &\text{Na}_1 (x:0.4520, y:0.2285, z:0.4333), \\ &\text{Na}_2 (x:0.9398, y:0.7382, z:0.3914), \\ &\text{O}_1 (x:0.1739, y:0.4749, z:0.3775), \\ &\text{O}_2 (x: 0.6950, y: 0.0102, z:0.3570) [11]. \end{aligned}$$

One Mn and one O atom was chosen to act as the photon absorber and the photoelectron emitter in each step's computations. Temperature calculations were done for 300 K, 323 K, 343 K, 373 K, and 423 K.

## 3. Results and discussion

The Mn K-edge and O K-edge atoms of the crystals were subjected to XAFS calculations in order to analyse the electronic characteristics and electronic interactions among the electrons of the neighbouring atoms as well as to shed light on background mechanisms in the  $\text{Na}_4\text{MnO}_4$  and  $\text{Li}_2\text{Na}_2\text{MnO}_4$  crystals. The spinel structure in the crystals is built by the metal manganese, and oxygen atoms are the essential ingredients that connect metals to one another, much like cementitious materials bind bricks together. In  $\text{Li}_2\text{Na}_2\text{MnO}_4$  crystals with different temperatures, Fig. 2 (a) compares calculated absorbance data from the K-edge of manganese atoms. The photon excitation process of 1s core electrons transitioning to the unoccupied 3d level as a final state produces Mn K-edge absorption spectra. The forbidden transition to the Mn 3d-O 2p hybridised state caused the absorption spectra to rise starting at 6535.26 eV and giving a weak but strong pre-edge peak at 6541.33 eV ( $t_{2g}$ ) and 6544.64 eV ( $e_g$ ). The strength of the Mn-O bonding in the  $\text{Li}_2\text{Na}_2\text{MnO}_4$  material is correlated with the pre-edge peak's sharp intensity. The Mn 4s and O 2p levels provide a weak pre-edge feature that resembles a shoulder at 6556 eV, which is located above the pre-edge peak of the dp hybridization. The prominent peak at 6564.82 eV on the main edge of the Mn K-edge spectra is the result of excited 1s electrons to vacant 4p levels. Both Fig. 1 (b) and Fig. 2 (a) make it evident that the manganese atoms in this structure have tetrahedral site symmetry and are connected to four oxygen atoms via their respective 3dxy, 3dyz, 3dzx, and 4s orbitals. Accordingly, the  $\text{Li}_2\text{Na}_2\text{MnO}_4$  material's temperature dependence is demonstrated to be stable. Fig. 2 (a) shows that the  $\text{Li}_2\text{Na}_2\text{MnO}_4$  material's temperature dependence is stable, and Fig. 2 (b) shows that the parent  $\text{Na}_4\text{MnO}_4$  material's temperature dependence is stable as well. The atomic symmetries have slightly changed because lithium atoms' valence orbitals differ from sodium atoms'. The peak for the parent material shows a slight decline at the sp hybridised peak on the major edge and a weak energy shift. The stable crystal structure of both the parent and the Li-substituted samples is confirmed by the high symmetry in the peak structure against rising temperature.

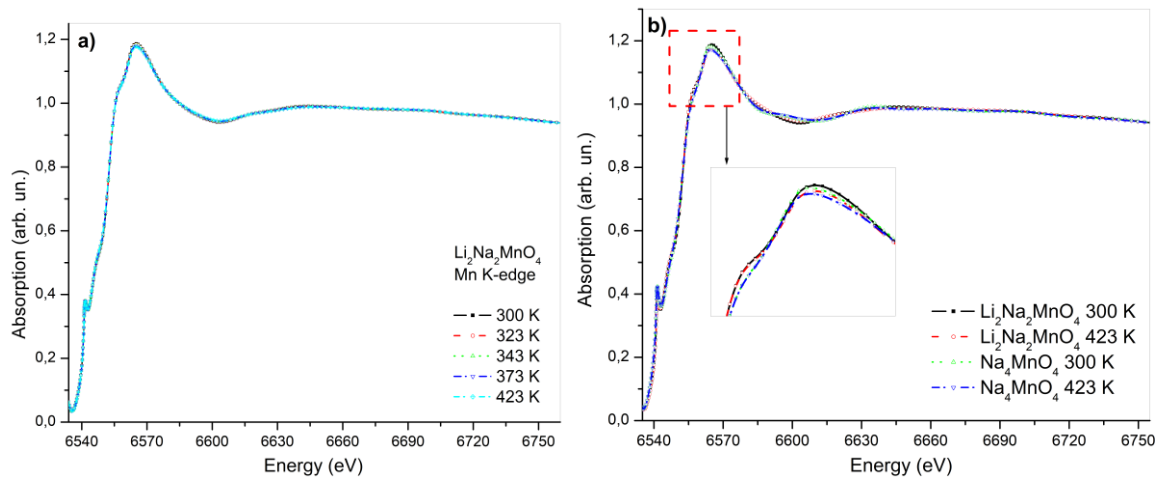


Fig. 2. (a) Comparison of Mn K-edge absorption spectra of  $\text{Li}_2\text{Na}_2\text{MnO}_4$  at 300 K, 323 K, 343 K, 373 K, and 423 K temperatures; (b) Mn K-edge comparison of  $\text{Li}_2\text{Na}_2\text{MnO}_4$  and  $\text{Na}_4\text{MnO}_4$  crystals at temperatures of 300 K and 423 K.

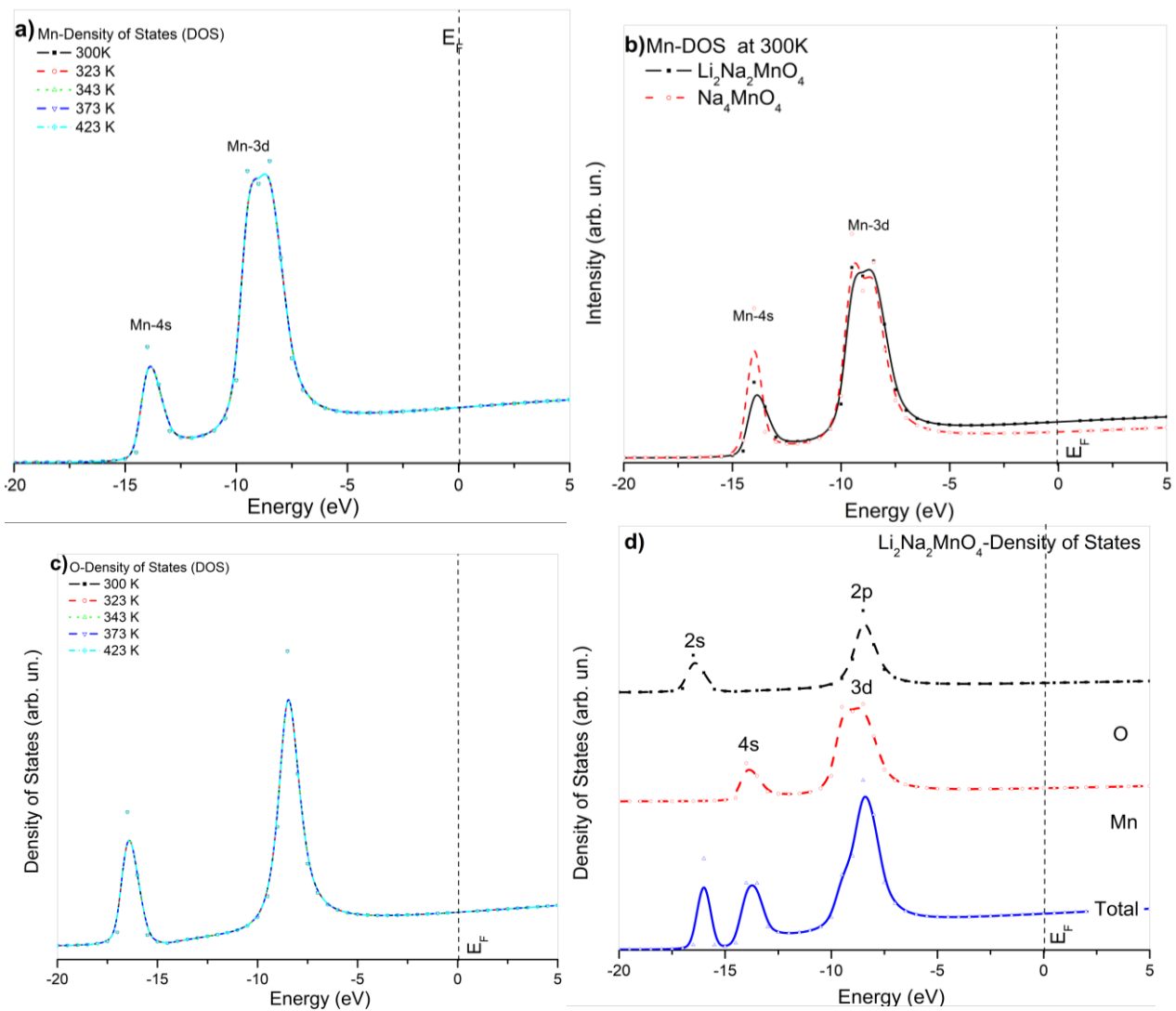


Fig. 3. (a) Mn DOS in  $\text{Li}_2\text{Na}_2\text{MnO}_4$  was compared at 300 K, 323 K, 343 K, 373 K, and 423 K; (b) Mn DOS comparison of  $\text{Li}_2\text{Na}_2\text{MnO}_4$  and  $\text{Na}_4\text{MnO}_4$  crystals at 300 K; (c) The DOS comparison of oxygen in  $\text{Li}_2\text{Na}_2\text{MnO}_4$  at 300 K, 323 K, 343 K, 373 K, and 423 K temperatures; (d) Total DOS of  $\text{Li}_2\text{Na}_2\text{MnO}_4$  at 300 K (color online)

The density of states (DOS) calculation seems to show the electronic interaction between nearby Mn and O atoms that leads to hybridised levels. The predicted DOS of the manganese atoms in the material is shown in Fig. 3 (a) and (b) it appears from Fig. 3 (a) that there was no change as the temperature increased, highlighting a remarkably stable electronic structure at and above room temperature. The primary orbitals for manganese have a wide range of energies up to 10 eV and are crucial for the bonding mechanism. The 4s level of manganese is positioned just beneath the 3d state. Due to its proximity energy to oxygen orbitals and potential to pair to bind with oxygen 2p levels, this level participates quite actively in electronic interaction as well. Fig. 3 (c) compares the DOS of oxygen atoms in the  $\text{Li}_2\text{Na}_2\text{MnO}_4$  material at various temperatures. Similar to the manganese orbitals, the oxygen states were unaffected by the rise in temperature above ambient levels up to 423 K. Despite the fact that manganese orbitals are stable, it was anticipated that changes to the Li or Na states would result in changes to their low ionic states as  $\text{Li}^+$  and  $\text{Na}^+$ , which also have lower electronegativity than manganese and weaker bonds with oxygen atoms. However, the stable orbitals with

relation to the rising temperature are so astounding that even in the Li and Na states, there is no change with the rising temperature. Both Li and Na ions are anticipated to separate from oxygen bonds in battery cathode materials when a voltage difference is applied.

Li and Na atoms are not affected by temperature changes, which is encouraging, but it also reveals firmly bound ions that are difficult to separate from oxygen, indicating that they cannot be utilized as cathodes.

In Fig. 3 (d), the total DOS of the  $\text{Li}_2\text{Na}_2\text{MnO}_4$  material is shown alongside the DOS of Mn and O at 300 K. The energies of Mn and O have merged in entire DOS, providing unequivocal proof that Mn3d and O2p have hybridised. This result also demonstrated the potency of the creation of a hybrid molecular band. To observe the projections of electronic interactions on the oxygen atoms in both  $\text{Li}_2\text{Na}_2\text{MnO}_4$  and  $\text{Na}_4\text{MnO}_4$  crystals, calculated O K-edge XANES data is shown. O K-edge comparisons versus conditions of rising temperature are shown in Fig. 4 (a) High symmetry in the spectra at various temperatures also supports the  $\text{Li}_2\text{Na}_2\text{MnO}_4$  material's stable electronic structure of oxygen atoms, which is seen in Fig. 3 (c) above.

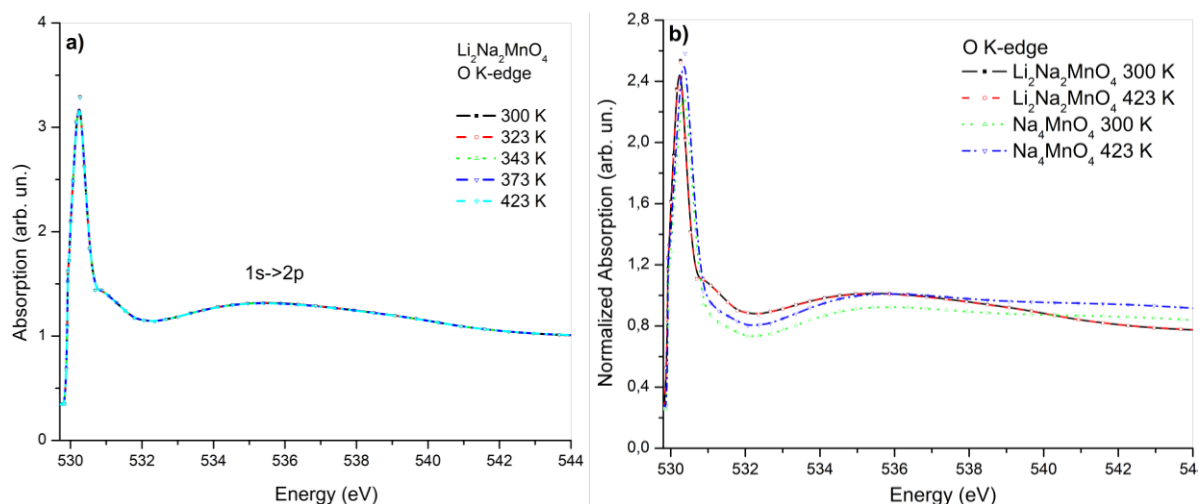


Fig. 4. (a) Comparison of O K-edge absorption spectra of  $\text{Li}_2\text{Na}_2\text{MnO}_4$  at temperatures of 300 K, 323 K, 343 K, 373 K, and 423 K; (b) Comparison of the O K-edge XANES spectra of  $\text{Li}_2\text{Na}_2\text{MnO}_4$  and  $\text{Na}_4\text{MnO}_4$  crystals at 300 K, and 423 K temperatures (color online)

The comparative spectra in Fig. 4 (a) have provided extremely valuable information regarding the electronic interaction near the oxygen atoms of the investigated sample. The transition of excited 1s core electrons to unoccupied states above the Fermi level as a final state, i.e.,  $1s \rightarrow 2p$ , is what creates the O K-edge. The Mn 3d-O 2p hybridised state caused the spectra to sharply peak at 529.77 eV as they began to rise. The number of vacant spaces in the final state affects the peak's strength and sharpness. Due to the Li 2s-O 2p hybridised state at 535.46 eV, a shoulder-like gaussian type pre-edge peak is present beyond the first pre-edge peak. It's interesting that no pre-edge peak has been seen—or one that is too faint to be seen—for a potential Na 3s-O 2p hybridization. A comparison of the O K-edge XANES spectra of  $\text{Li}_2\text{Na}_2\text{MnO}_4$  and  $\text{Na}_4\text{MnO}_4$  crystals at 300 K and 423 K is

shown in Fig. 3 (b). Li presence makes a very slight shift toward the lower energy side visible, which was also visible with the pre-edge peak in Li containing material. The impulse between the 2p levels of oxygen and sodium, where the accessible 2s levels of sodium are located, is another reason why the second pre-edge peak (Li-O) in  $\text{Na}_4\text{MnO}_4$  crystal has vanished. The evidence supports a strong link between lithium and oxygen atoms, but not sodium and oxygen.

Fig. 5 (a), in contrast, displays scattering data that was taken from the extended part of the XAFS data (EXAFS), which was produced from fluctuations at the tail section of the spectra. The scattering mechanism of the photoelectrons released from the source atom is what causes the oscillations in the tail portion of the XAFS spectra. The scattering peaks have varying strengths due to

the heterogeneous environment in which the source Mn atom is positioned, highlighting nearby atoms with extremely differing atomic weights. The photoelectrons' kinetic energy decays as they move between nearby atoms, which influences intensity. The photoelectron travels through regions of interstitial potential, where inhomogeneous potentials result to higher decay rates than regions of homogeneous potential. High symmetry in the comparison of the scattering intensities attests to the

atomic coordinations surrounding the source manganese atoms' high resistance to temperature increases. However, a degradation has been seen concurrent with the temperature rise. The amount of outer shell electrons that balance out the entering photoelectrons determines the rate of decay. In fact, the stability highlights the electrochemical properties that are less strong while highlighting the thermoelectric features [12].

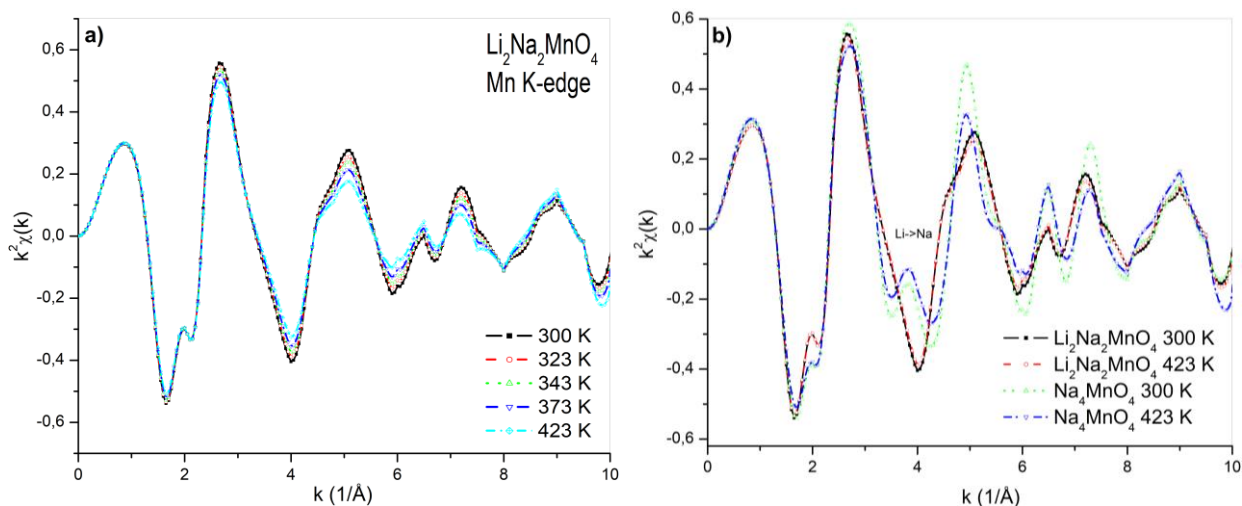


Fig. 5. (a) EXAFS scattering data comparison of  $\text{Li}_2\text{Na}_2\text{MnO}_4$  material at temperatures of 300 K, 323 K, 343 K, 373 K, and 423 K; (b) A comparison of the scattering intensities of  $\text{Li}_2\text{Na}_2\text{MnO}_4$  and  $\text{Na}_4\text{MnO}_4$  crystals at 300 K, and 423 K, respectively (color online)

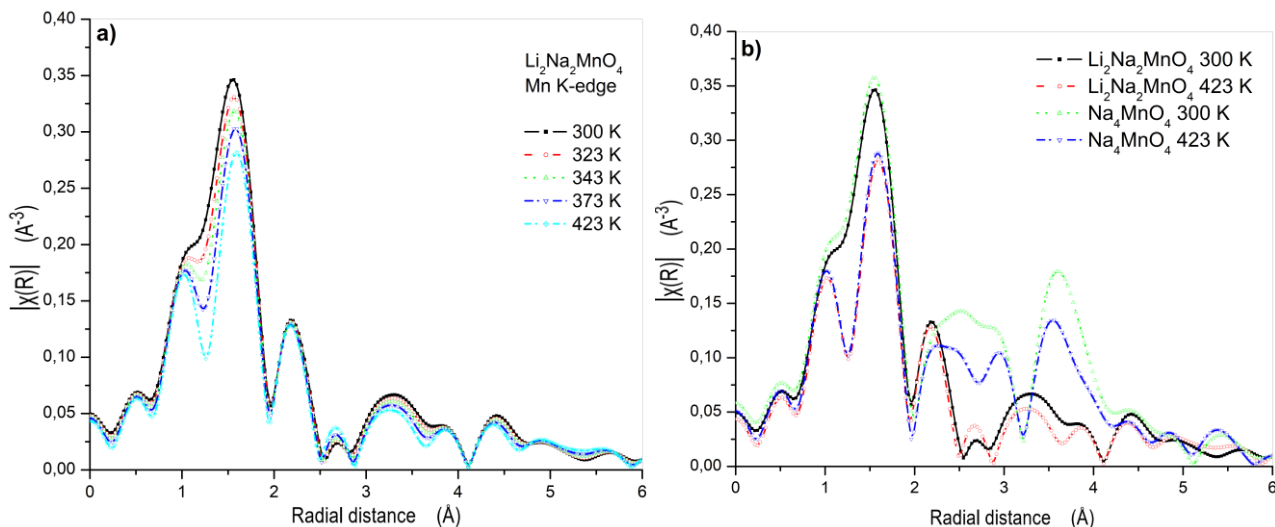


Fig. 6. (a) FT-EXAFS data comparison of  $\text{Li}_2\text{Na}_2\text{MnO}_4$  material at temperatures of 300 K, 323 K, 343 K, 373 K, and 423 K; (b) A comparison of the FT-EXAFS data of  $\text{Li}_2\text{Na}_2\text{MnO}_4$  and  $\text{Na}_4\text{MnO}_4$  crystals at 300 K, and 423 K (color online)

Fig. 5 (b) compares the scattering intensities of crystals made of  $\text{Li}_2\text{Na}_2\text{MnO}_4$  and  $\text{Na}_4\text{MnO}_4$  at 300 K and 423 K. With a high rate of signal degradation, lithium atom scattering intensities are plainly visible. A longer mean free path for the photoelectrons is supported by the intensities being correlated with the atomic weights of the materials and the presence of greater uniformity. In addition, the parent material,  $\text{Na}_4\text{MnO}_4$ , showed extremely high decay when compared to  $\text{Li}_2\text{Na}_2\text{MnO}_4$ , which points out possible better thermoelectricity.

The real-space atomic locations and distances from the source (Fe) atoms are provided by the Fourier transform of the scattering data taken from the XAFS data (FT-EXAFS), and this may be the best representation of the atoms during temperature change. Fig. 6 (a) compares  $\text{Li}_2\text{Na}_2\text{MnO}_4$  at various temperatures using FT-EXAFS data. For the analyses Athena and Artemis from the Demeter package Iffeffit pack was used to calculate the radial distances [5]. The  $\text{Li}_2\text{Na}_2\text{MnO}_4$  material's closest surrounding atom shell's positions and separations from

the source Mn atom were established by analysis. The analysis shows that two oxygen atoms (Mn-O) are the nearest atoms to the manganese atoms. The next closest neighbours are sodium atoms and lithium atoms, which are located at various distances as follows: one Na atom is located at 2.986 Å, one Li atom is located at 3.011 Å. It was discovered that the manganese atom that was closest to the source manganese atom was located at a distance of 4.956 Å. The analysis shows that two oxygen atoms (Mn-O) are the nearest atoms to the manganese atoms. The next closest neighbours are sodium atoms and lithium atoms, which are located at various distances as follows: one Na atom is located at 2.986 Å, one Li atom is located at 3.011 Å, and one Na atom is located at 3.110 Å. It was discovered that the manganese atom that was closest to the source manganese atom was located at a distance of 4.956 Å.

The lithium replaced sample exhibits the same unambiguous decay with temperature increase as in Fig. 6.a, and as a validation of the stability as stated above, the peak positions exhibit good symmetry with no shifts. The parent oxide material,  $\text{Na}_4\text{MnO}_4$ , showed more degradation when compared to the FT-EXAFS data of  $\text{Li}_2\text{Na}_2\text{MnO}_4$  at 300 K and 423 K in Fig. 6 (b). The stable crystal structures of both parent and lithium substituted materials against conditions of rising temperature are addressed by the high agreement on the peak structures. The FT-EXAFS strongly demonstrated that neither the sodium atoms nor the substituted lithium atoms moved from their positions in the crystal as the temperature increased. This is good for the material's ionic conductivity, which is important in batteries because heat is released from the cathode materials during intercalation processes, which degrades performance. On the other hand, ionic conductivity in a battery cathode is an issue caused by closely bound oxygen atoms, which should be managed with applied voltage.

#### 4. Conclusions

To investigate the ionic properties at 300 K, 323 K, 343 K, 373 K, and 423 K temperatures, lithium substituted  $\text{Na}_4\text{MnO}_4$  materials ( $\text{Li}_2\text{Na}_2\text{MnO}_4$ ) and their electronic and crystal structure properties were examined. The main objective of the study was to examine how their structural characteristics changed as the temperature rose and to ascertain whether or not they met the requirements for battery cathodes. Studies on the electronic structure have shown that lithium substituted compounds and their parent materials both exhibit a stable electronic structure at high temperatures. Due to the intercalation mechanism, the close binding of metals with oxygen atoms can cause issues with cathodic characteristics. Although the examined materials lacked the necessary characteristics to serve as a battery cathode, high electronic data loss with rising temperature circumstances suggested potential for good thermoelectric performances at room temperature with an unaffected, stable crystal structure.

#### References

- [1] K. Chayambuka, G. Mulder, D. L. Danilov, P. H. L. Notten, *Adv. Energy Mater.* **8**, 1800079 (2018).
- [2] O. M. Ozkendir, *Materials Today Communications* **24**, 101241 (2020).
- [3] J. Zhao, L. Zhao, N. Dimov, S. Okada, T. Nishida, *Journal of the Electrochemical Society* **160**(5), A3077 (2013).
- [4] D. Susanto, M. K. Cho, G. Ali, J.-Y. Kim, H. J. Chang, H.-S. Kim, K.-W. Nam, K.-Y. Chung, *American Chemical Society* **31**(10), 3644 (2019).
- [5] A. L. Ankudinov, B. Ravel, J. J. Rehr, S. D. Conradson, *Phys Rev B.* **56**, R1712 (1990).
- [6] K. Momma, F. Izumi, *J. Appl. Cryst.* **44**, 1272 (2011).
- [7] O. M. Ozkendir, Y. Ufuktepe, *J. Optoelectron. Adv. M.* **7**(5), 2655 (2005).
- [8] O. M. Ozkendir, *Lab-in-Silico* **1**(2), 1 (2020).
- [9] M. Newville, *J. Synchrotron Rad.* **8**, 322 (2001).
- [10] O. M. Ozkendir, *Advanced Journal of Chemistry, Section B-Natural Products and Medical Chemistry* **2**(2), 48 (2020).
- [11] A. Jain, S. P. Ong, G. Hautier, W. Chen, W. D. Richards, S. Dacek, S. Cholia, D. Gunter, D. Skinner, G. Ceder, K. A. Persson, *APL Materials* **1**, 011002 (2013).
- [12] O. M. Ozkendir, H. Miyazaki, S. Gunaydin, *J. Electron. Mater.* **51**, 1740 (2022).

\*Corresponding author: ozkendir@tarsus.edu.tr